



2013

On Development of Autonomous HAHO Parafoil System for Targeted Payload Return

Benton, J.E.

Monterey, California: Naval Postgraduate School

þÿ[Snowflake] Benton, J.E., and Yakimenko, O.A., On Development of Aut



Calhoun is a project of the Dudley Knox Library at NPS, furthering the precepts and goals of open government and government transparency. All information contained herein has been approved for release by the NPS Public Affairs Officer.

Dudley Knox Library / Naval Postgraduate School
411 Dyer Road / 1 University Circle
Monterey, California USA 93943

On Development of Autonomous HAHO Parafoil System for Targeted Payload Return

Joshua E. Benton*

San Jose State University, San Jose, CA, 95192-0087

Oleg A. Yakimenko[#]

Naval Postgraduate School, Monterey, CA 93943-5107

An autonomous HAHO (high altitude, high-opening) parafoil system design is presented as a solution to the final descent phase of an on-demand International Space Station (ISS) sample return concept. The system design is tailored to meet specific constraints defined by a larger study at NASA Ames Research Center, called SPQR (Small Payload Quick-Return). Building on previous work in small, autonomous parafoil systems development, a SPQR-compatible evolution of an existing advanced parafoil delivery system is designed, built, and test-flown deployed from unmanned air vehicles and high-altitude balloons. Results of the preliminary tests of the original and SPQR-compatible systems are presented, and applicability of the test article to actual spaceflight conditions is discussed.

I. Introduction

The motivation for this project is led by the development of SPQR study intended to routinely deliver small payloads from ISS on-demand. The first successful recovery of an object from orbit occurred under the US's top-secret CORONA spy satellite program. This program operated from 1959 to 1972, existing primarily as a means to keep a watchful eye on the nuclear weapons progress of the Soviet Union. The satellites used by CORONA carried highly-advanced film camera systems which snapped surveillance photographs from orbit, and the film was then returned by a reentry capsule and parachute system. A small decelerator parachute deployed as high as 65,000ft (19,812m) altitude, and a main chute was deployed 10,000ft (3,048m) lower. Finally, the entire film "bucket" and parachute were snatched from the air by a large, specially-equipped Air Force airplane.¹

With the growth of the US space program during the same era, the use of parachutes to safely return space payloads on their final stages of descent became commonplace. The manned Mercury, Gemini, and Apollo capsules used parachute recovery systems as well. Currently, modern space missions (manned, such as the Russian Soyuz capsule, or unmanned, such as SpaceX Dragon) frequently make use of parachutes for slowing their payload's final atmospheric descent.

The SPQR concept, originating from NASA Ames Research Center at Moffett Field, CA, relies on a three-stage method of returning payloads, after being stored until needed and then loaded while on-board the ISS (Fig.1):

- Deorbit, by means of a passive deployable drag system,
- Atmospheric reentry, via the deployment of a passively self-stabilizing reentry body,
- Terminal descent of the temperature-controlled payload canister beneath an autonomous guided parafoil, following the shedding of the reentry aeroshell.²

The first two return phases exist at varying levels of maturity. The passive drag deorbit system has yet to be tested in a space-like environment, but the self-stabilizing reentry vehicle has undergone multiple successful flight tests as a series of sounding rocket payloads.³ The third and final phase, terminal guided descent, is where the focus of this project lay. To mature this final phase of the SPQR concept, an autonomous parafoil system which satisfies the demands of the volumetric, environmental (space-flight), and landing precision requirements must be developed.

A handful of autonomous parafoil systems exist and their guidance routines are highly refined (though also proprietary),⁴ but none of these available systems completely satisfies the specific set of unique challenges and

* Currently, Aerospace Engineer, Small Spacecraft, NASA Ames Research Center, joshua.benton@nasa.gov, Member AIAA.

[#] Professor, Department of Systems Engineering, Code SE/Yk, oayakime@nps.edu, Associate Fellow AIAA.

requirements imposed by the SPQR design scenario. The miniature payload delivery system Snowflake,⁵ developed by the University of Huntsville in Alabama and the Naval Postgraduate School in California, happens to be the closest candidate for prototyping the SPQR-compatible system. It utilizes a parafoil approximately six feet (1.83m) in span when inflated (with two other options: nine feet (2.74m) and twelve feet (3.66m) in span also available), capable of carrying about 10lbs (4.54kg) payload (up to 30lbs for the larger versions of the canopy) and relies on a guidance, navigation and control (GNC) electronics unit roughly the size of a deck of cards.^{5,6} What is even more attractive is its particularly advanced open-source targeting algorithm, enabling landing accuracies of 10m circular error probable (CEP).⁶ These extreme levels of precision are accomplished by real-time generation of flight trajectories by the Snowflake's GNC system, which updates flight parameters based on wind estimations and atmospheric conditions in its descent, as well as optimizing the final up-wind turn as it is being executed to ensure both a soft and precise landing.⁷ Snowflake's control algorithms also accommodate the wind profiles (when available),⁸ which will be one of the most critical features for SPQR.



Fig 1. Pictorial overview of SPQR on-demand payload delivery system concept, from ISS deployment to atmospheric descent.

In addition, a scalable version of the parafoil system like Snowflake would have many other aerospace applications beyond the SPQR system, including, for example, greatly simplified retrieval of sounding rocket payloads. At present, such payloads launched from NASA's Wallops Flight Facility typically rely on recovery from the ocean by small fishing vessels (if they are to be recovered at all), which is time-consuming, inefficient, and occasionally unsuccessful. Sounding rockets provide a relatively inexpensive means to test small payloads in a space environment, but the additional cost of telemetry and communications, and the difficulty of recovering payloads, make them far less attractive for deployable experiments. A reliable precision return system for deployable payloads could make on-board data logging a feasible alternative to expensive ground-based communications, and significantly reduce the associated costs of sounding rocket experimentation. Also, on-board logging can record an enormous quantity of data at very high bitrates, enabling greater experiment precision if the data has a high probability of being recovered.⁹

A further application of a miniature, lightweight, autonomous parafoil system is the increasingly-common use of high-altitude weather balloons for amateur experimenters. Balloon payloads routinely carry parachutes for safe recovery after the bursting of the balloon, but the final landing spot of the payload is at the mercy of the winds it encounters on descent. Typically, the recovery of the payload is the most challenging aspect of balloon experimentation, and losing a payload in an unexpected landing location is not at all a rare occurrence. If the standard payload return parachute was replaced with a very small, autonomous guided parafoil system, payloads could be returned to a pre-defined location and eliminate the elaborate routine of chase vehicles and search crews that accompany most balloon launches.

The objectives of this multi-faceted research addressed in this paper were as follows:

- 1) Re-design and miniaturize an existing autonomous parafoil control system and its associated control line rigging to fit within the volumetric constraints of the SPQR payload canister.
- 2) Develop new autonomous control software to steer and land the parafoil at a target GPS coordinate on the ground from any starting point, requiring only the target coordinates and target elevation as inputs.

- 3) Verify the performance of the new control system hardware and software via flight testing from an altitude sufficient to determine control characteristics, and demonstrate the ability of the system to manage flight disturbances such as crosswinds.
- 4) Discuss strategies to enable the use of the parafoil system in a challenging space-purposed scenario, including design considerations to ensure compatibility with ISS safety protocol.

The ultimate goal of this project would be a complete, functional prototype of an autonomous parafoil return system, compatible in size, shape, mass, and method of operation with the SPQR sample return canister.

Up to date several dozens of low-altitude and seven high-altitude deployments of the two versions of the proposed systems in support of a broader SPQR project were conducted, and even though not all objectives have yet been met this paper presents the current status and is organized as follows: Section II overviews the results of the preliminary high-altitude tests accomplished over the period of two years, 2010-2011, with the goal of better understanding all the challenges of a low-stratosphere deployment of a ram-air parachute system. Section III addresses the issue of estimating the descent time needed for the system design. Section IV discusses design considerations for the full-fledged SPQR-ready system and presents a prototype of such a system. Section V provides a brief discussion of challenges associated with a control of a parafoil system over a large spread of flying conditions while Section VI outlines the initial flight test results of the developed SPQR-compatible prototype.

II. Preliminary Design and Trial High-Altitude Drops

The first version of the proposed system (System A) was largely based on the existing Snowflake design (Fig.2). In its first design iteration, a basic facsimile of the Snowflake's mechanical systems was fabricated, and a new control board was implemented for the GNC with a goal of utilizing a very simple steering algorithm to serve as a basic prototype needed to obtain some high-altitude drop test data for further redesign. This basic algorithm reads the GPS heading from the control board, compares it to a predefined heading that it is programmed to follow, and then computes a control command of fixed magnitude to steer right, left, or straight.

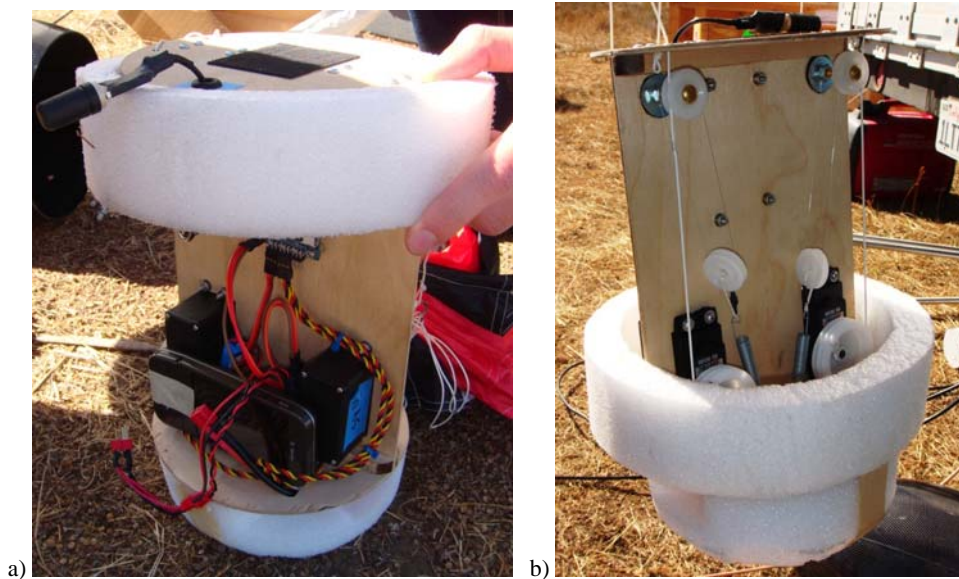


Fig. 2. System A design (Snowflake's facsimile).

First, the basic simple-control System A was tested in multiple air-drops from a UAV at altitudes up to 3,000ft (914m) AGL at Camp Roberts, CA. These drops were generally successful with rapid parafoil deployment and inflation, and the device maintained the correct heading throughout its descent. Having demonstrated basic system performance and the ability to fly toward a pre-specified heading with the UAV drops, the next goal was to determine the flight characteristics of the parafoil over a much greater altitude range - approximately 50,000ft (15,240m) to ground level. Because the SPQR parafoil system is intended to provide final trajectory correction for a payload returned from orbit, the maximum trajectory correction possible will be achieved by deploying the parafoil at as high an altitude as possible.

The high-altitude testing was carried out in Idaho and Washington (Fig.3), with the help of the University of Idaho's Vandal Atmospheric Science balloon Team (VAST). Four balloon flights (10/16/10, 4/23/11, 8/19/11, 10/13/11) were conducted with the System A device, with varying levels of success. For every flight, high-definition

(720p, 60fps) video was captured with up-looking and 45° down-looking video cameras, data were logged by the Ryan Mechatronics Monkey control board (with full data logging of component velocity, spatial location, three-axis acceleration, UTC time, servo steering commands, flight heading, and more), and the parafoil system was tracked via the Automatic Packet Reporting System (APRS) amateur radio network to facilitate recovery.



Fig. 3. Above the clouds: a view over eastern Washington, near the Idaho border, from the balloon's perspective.

During the first balloon flight test on Oct. 16, 2010, the parafoil system failed to separate from the balloon, even though it can be seen and heard on the on-board video that the separation charge fired as expected at altitude. Also, no visible tangles were present in the shroud lines, so the exact reason for the parafoil system not separating is still unknown. Because separation from the balloon never occurred, the entire payload was lifted to burst altitude with the balloon (approximately 80,000ft (24,384m)). The instant of balloon burst is shown in Fig.4a.

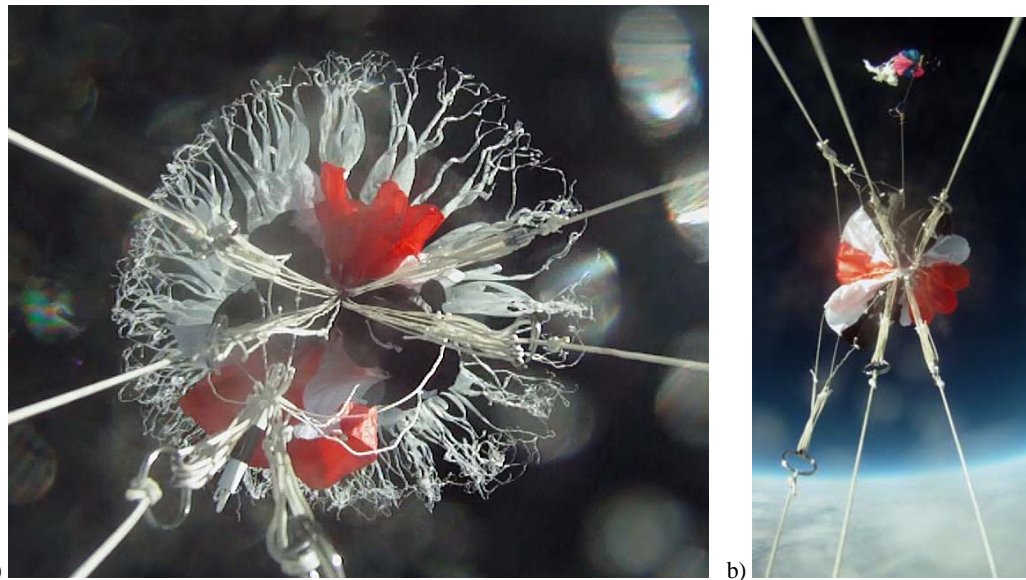


Fig. 4. Balloon at the instant of burst viewed from on-board video camera after a failed release (a); the tangled parafoil co-orbits the steering system in a flat spin (b).

Upon burst, the combined package of parafoil system, balloon tracking system, and attachment lines began a rapid flat-spin, and the tangled system fell to the ground in this state. Figure 4b shows the system following balloon burst, with the parafoil and payload co-orbiting one another on a plane nearly parallel to the ground.

During the second balloon flight test on April 23, 2011, the system was successfully deployed from the balloon at approximately 35,000ft (10,668m) altitude. However, upon release, the video data shows that the parafoil inflated only partially. It can be seen in the video that the riser line bridle constricted the parafoil from opening fully, despite the bridle not being tangled in any way (Fig.5). In this state, the system was uncontrollable and descended in a high-

velocity spiral. After reaching approximately 10,000ft (3,048m) altitude, the parafoil finally inflated completely, and nominal flight began. Figure 6 shows the flight track of the system from the on-board GPS log. The parafoil system was programmed to fly a fixed heading of 270° (due west). The ground-track of the system is indicated by the projected shadow in Fig.6. Examining this ground track, one can easily see the point at which the parafoil inflated and began flying the due west heading.

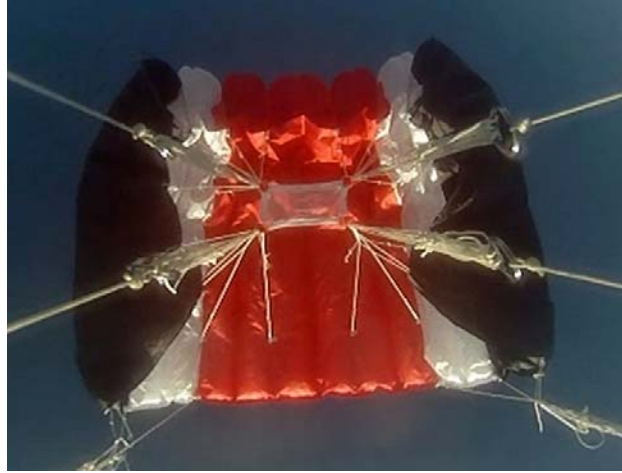


Fig. 5. Partially-inflated parafoil and elevated bridle resulting in loss of control during first 23,000ft (7,010m) of descent.



Fig. 6. GPS-logged flight track of System A.

Based on the flight video, it was speculated that the parafoil bridle created excessive frictional resistance for the parafoil to fully inflate at high altitudes and low atmospheric density. Dynamic pressure is diminished even further in the balloon drop scenarios due to the gentle release of the system from the balloon, with no significant forward velocity. A bridle is typically present on parachutes and parafoils to moderate the rate of inflation, thus easing the deceleration forces on the passenger or payload. This is of no practical value from a gentle balloon release with an already-deployed canopy, so it was decided to simply remove the bridle for the next balloon flight test.

After conducting several low-altitude drop tests of the parafoil system without the bridle (to ensure that the removal of the bridle did not adversely affect the flight characteristics or steering performance of the parafoil), another balloon flight was attempted on Aug. 19, 2011. Again, the parafoil cut-away from the balloon worked as planned, at approximately 35,000ft (10,668m) altitude. As in the previous flight, despite absolutely nominal release conditions, the parafoil failed to inflate. The video data shows the parafoil falling gently away from the balloon and immediately collapsing upon itself (much like it might in vacuum), and the whole system quickly enters a high-yaw-rate flat spin. Figure 7a shows System A a moment after release, with the balloon drifting away, and the parafoil already collapsed into a loosely crumpled mass. Unlike the previous flight, where the parafoil eventually inflated

and recovered, the crumpled parachute system continued in a rapid flat-spin all the way to the ground. Figure 7b shows the view of the collapsed parafoil from the on-board camera during this energetic flat-spin.

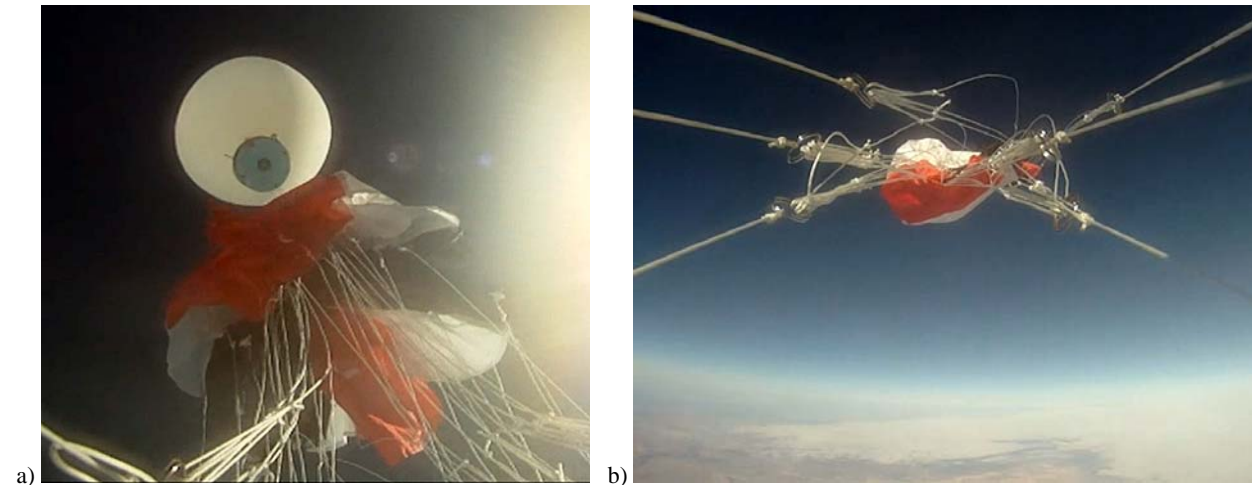


Fig.7. Immediate collapse of parafoil following balloon separation (a); flat spin resulting from collapsed parafoil proves to be unrecoverable (b).

All balloon flights prior to this test encountered partial or total failures due to delayed or failed parafoil inflation. Based on the video data, it appeared that the lack of inflation was caused by several factors: low atmospheric density at altitude, resulting in diminished dynamic pressure and less total drag to inflate the parafoil cells and keep the parafoil above the payload; lack of forward velocity upon release from the balloon, also causing diminished dynamic pressure to inflate the parafoil cells; and the initial collapsed state of the parafoil upon release, which inhibits air flow into the parafoil cells and makes inflation exceedingly difficult in the high altitude, low density release regime.

To aid the parafoil's inflation, a system of flexible carbon fiber support rods was attached to the top of the parafoil canopy, giving it a small but significant degree of structural support, while still preserving the parafoil's ability to flex and deform as necessary for steering. The carbon fiber stiffening structure, shown in Fig.8a works much like a simple dome tent. The length of the carbon fiber rods that cross the top of the parafoil are slightly longer than the distance across the parafoil where they attach, and thus they are subjected to a compressive buckling state when attached to the parafoil. This results in a parafoil that is capable of maintaining its basic curvature while suspended under its own weight (Fig.8b), without being so rigid as to inhibit normal flight characteristics.



Fig. 8. Parafoil stiffening structure test-fitted to parafoil (a), suspended parafoil remains open, yet highly flexible under its own support (b).

This semi-rigid parafoil was flown in the fourth balloon test at Idaho on Sept. 13, 2011. The intention of the test was to gather data for a “best-case scenario” of parafoil inflation at a very high altitude (approximately 50,000ft (15,240m)), and record the parafoil flight performance characteristics in great detail through on-board data logging. By supporting the shape of the parafoil with the structure, the tendency for the parafoil to collapse was eliminated, and the structure also helped to keep the parafoil cell entrances open, aiding inflation.

Figure 9a shows the parafoil maintaining its shape beneath the balloon shortly after release by the ground crew at about 42,000ft (12,802m) altitude. The top portion of Fig.9b attests that the parafoil cells inflated fully immediately upon separation. However, due to a shroud line snag that occurred prior to the balloon being released from the ground, the left side of the parafoil was deformed and, again, a spiraling flat-spin ensued. Unfortunately, the system continued this spiral until only 3,000ft (914m) above ground level, at which point a sharp “snap” can be heard and seen in the video. The snagged line is then suddenly released, the uncontrollable spiraling immediately ceases, and the system flies nominally for a short time until landing (Fig.9b bottom).

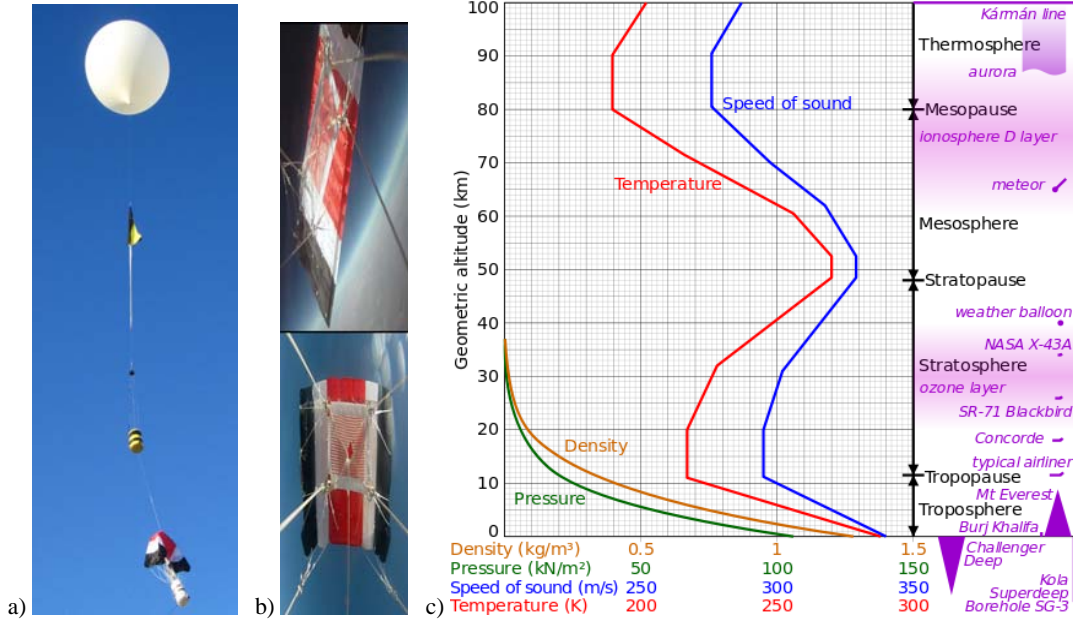


Fig.9. Rigidized parafoil maintaining its shape beneath a balloon payload train (a); a line snag causing an uncontrollable spiral (b, top); rigidized parafoil in nominal flight (b, bottom); parameters of the standard atmosphere (c).

To summarize the preliminary tests, it was expected that a ram-air parachute, by its self-inflating nature, will not perform well with low dynamic pressure. Because atmospheric density decreases as a function of altitude (Fig.9c), there is a threshold beyond which the SPQR system parafoil will not be operable. However, in those four balloon tests it was demonstrated that there is even a greater challenge of actually getting the parafoil to inflate at all. If the parafoil fails to inflate upon initial release at high altitude, tumbling and tangling occur almost immediately, thus preventing the parachute from inflating even after it descends into the lower, denser atmosphere. Tracking performance data collected during the preliminary tests also revealed a strong dependence from altitude, hence suggesting introducing a gain scheduling technique. Finally, the many challenging aspects of designing a system for spaceflight scenarios must be considered. Many of aforementioned concerns were addressed in the design of the SPQR-ready version parafoil descent system as described in Section IV, but before proceeding, the issue of estimating the descent time will be briefly addressed.

III. Estimation of the Descent Time

One of the goals of the preliminary high-altitude testing was estimating a time to descent from a certain altitude, or in other words, establishing the effect of air density ρ and perhaps mass of the system, m , onto its decent rate V_d .

Consider a quasi steady-state motion in the vertical plane

$$\frac{1}{2} C_L \rho V_d^2 S \approx mg \quad (1)$$

where C_L is the lift coefficient.

For the troposphere drops (from a UAV) we may assume that the atmosphere holds properties of the standard atmosphere model below 11km

$$\rho(H) = 1.225(1 - 0.00002256H[m])^{4.2559} \text{ [kg / m}^3\text{]} \quad (2)$$

where altitude H is measured with respect to the mean sea level. For example, according to Eq.(2), at 300m elevation (drop zone elevation) $\rho_{0.3} = 0.97\rho_0$ and at the release altitude of 3km MSL $\rho_3 = 0.74\rho_0$. How does this affect the descent rate?

Suppose we know the that with a nominal mass m^* the descent rate of some payload delivery system at the sea level ($H = 0$) is V_d^* . Then, rewriting Eq.(1) as

$$\rho V_d^2 = \frac{2mg}{C_D S} = const \quad (3)$$

yields

$$\rho_0 V_d^{*2} = \rho_H V_d^2 \quad (4)$$

or

$$V_d = \sqrt{\frac{\rho_0}{\rho_H}} V_d^* \quad (5)$$

Hence, $V_{d0.3} = 1.02V_d^*$ and at the release altitude of 3km MSL $V_{d3} = 1.16V_d^*$. What about the time of descent? Starting off the obvious relation

$$\frac{dH}{dt} = V_d \quad (6)$$

we arrive at

$$T = \frac{1}{V_d^*} \int_0^{H_d} \sqrt{\frac{\rho_H}{\rho_0}} dH \quad (7)$$

where H_d is the altitude of canopy deployment. For the low altitude drops (assuming a standard atmosphere described by Eq.(2)) Eq.(7) reduces to

$$T = \frac{1}{V_d^*} \int_0^{H_d} (1 - 0.00002256H)^{-2.1208} dH = -14171 \frac{1}{V_d^*} \left((1 - 0.00002256H_d)^{3.1208} - 1 \right) \quad (8)$$

Figure 10 shows this dependence for a nominal descent speed of 1m/s (3.3ft/s). As seen at low altitudes this dependence is almost linear so that the deployment altitude may be treated as AGL altitude. Also shown in the figure is the descent time based off the simple linear model

$$T = \frac{H_d}{V_d^*} \quad (9)$$

Obviously, for these altitudes the difference may be neglected (e.g., for our example of canopy deployment at 3km and drop zone altitude of 300m the difference between the models described by Eq.(8) and Eq.(9) is only about 6.5%).

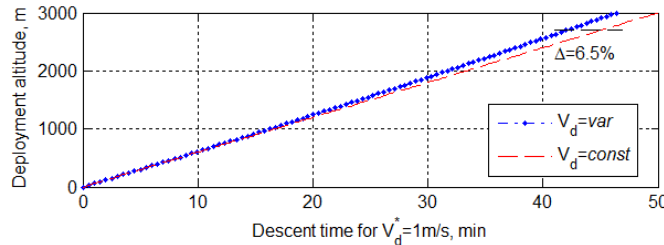


Fig. 10. Descent time T for a nominal descent rate of 1m/s versus a deployment altitude (in the troposphere).

For the stratospheric drops, we should account for two additional density models (Fig.9c). Along with Eq.(2), which is valid for $H \leq 11km$ we need to add a model for the tropopause $H \in [11; 20]m$

$$\rho(H) = 0.364 \exp(1.7346 - 0.0001577H[m]) [kg / m^3] \quad (10)$$

and the lower stratosphere $H \in [20; 32]m$

$$\rho(H) = 0.0880345(0.9077 + 0.000004616H[m])^{-35.163} [kg / m^3] \quad (11)$$

To avoid having a bulky expression for the time of descent, for our purposes we may also use a single exponential regression for the descent rate DR as shown in Fig.11.

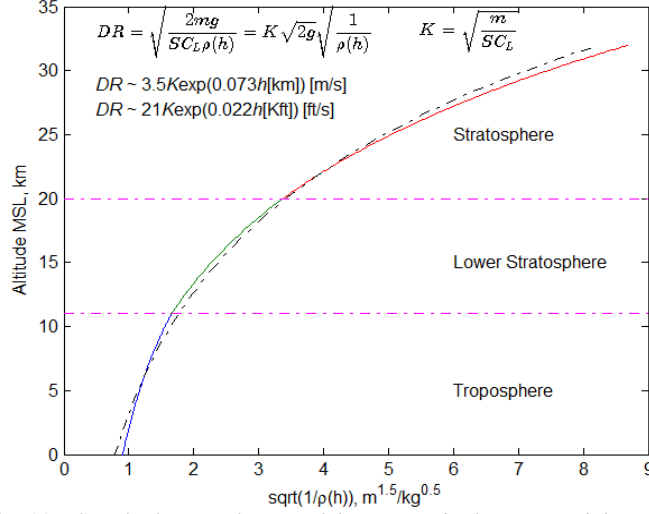


Fig. 11. Standard atmosphere model versus a single exponential model.

With this model Eq.(6) yields

$$T = \frac{1}{V_d^*} \int_0^{H_d} e^{-0.000073H} dH = -13700 \frac{1}{V_d^*} (e^{-0.000073H_d} - 1) \quad (12)$$

Figure 12 represents this dependence for a nominal descent speed of 1m/s similarly to that of Fig.10. Clearly, the linear model (9) for the stratosphere drops yields a huge error.

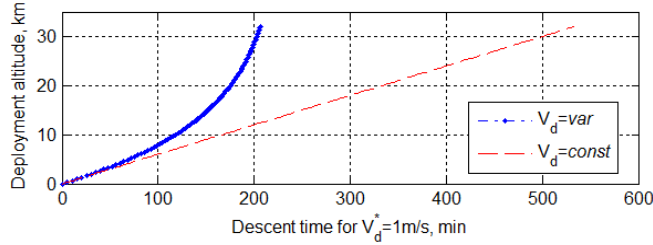


Fig. 12. Descent time T for a nominal descent rate of 1m/s versus a deployment altitude (in the lower stratosphere).

The estimate of the descent time obtained using Eq.(12) happened to be very close to the actual descent time in the last of four preliminary high-altitude drops.

To conclude this section, consider the following. Expressing Eq.(1) as

$$V_d = \sqrt{\frac{2mg}{C_L \rho S}} = \rho^{-0.5} const \quad (13)$$

and taking its variation yields

$$\delta V_d = -0.5 \delta \rho \rho^{-1.5} const \quad (14)$$

Next, dividing Eq.(14) by Eq.(13) arrives at

$$\frac{\delta V_d}{V_d} = -0.5 \frac{\delta \rho}{\rho} \quad (15)$$

Therefore, a 10% decrease in air density leads to a 5% increase of the descent rate.

Performing a similar analysis of the effect of the varying mass leads to the following:

$$V_d = m^{0.5} const \quad (16)$$

$$\frac{\delta V_d}{V_d} = 0.5 \frac{\delta m}{m} \quad (17)$$

Hence, the 10% increase in mass leads to a 5% increase of the descent rate (and 5% decrease of the descent time T).

IV. Design of SPQR-Ready System

Applied to the SPQR concept, there are a number of factors influencing the mechanical design of the complete parafoil return system which must be considered. These include physical shape and size, minimization of mass to the greatest extent possible, deployment considerations for the parafoil and GPS antenna, the operational environment of the device from launch to return (e.g. thermal and vacuum), and additional specific constraints that would be imposed by safety standards for transportation to (and stowage within) the ISS.

Though very compact compared to most existing autonomous parafoil return systems, the current Snowflake control system architecture and the prototype System A are both physically larger than the entire volume available for the control system and stowed parafoil inside SPQR. This is mainly attributable to the fact that both are development units, and durability, ease-of-assembly, and internal access for test modifications were of greater concern than packaging optimization. Because of this, there is significant potential for volumetric reduction.

A. General Design Considerations

Figure 13 shows the SPQR high altitude balloon-configured System A alongside the available volumetric envelope for the entire system, including the parafoil, within the SPQR payload canister (images are to scale). The payload canister (14.6cm (5.75”) in diameter and 17.93cm (7”) tall) is an insulated, thermally-controlled, pressurized module intended to accommodate a 3U-equivalent payload (approximately 10cm x 10cm x 30cm) in its pressurized volume, as well as the parafoil return system in the end opposite the payload. This canister assembly, called the Payload Containment and Thermal Control Unit (PCTCU), was developed by Paragon Space Development Corporation of Tucson, Arizona.¹⁰

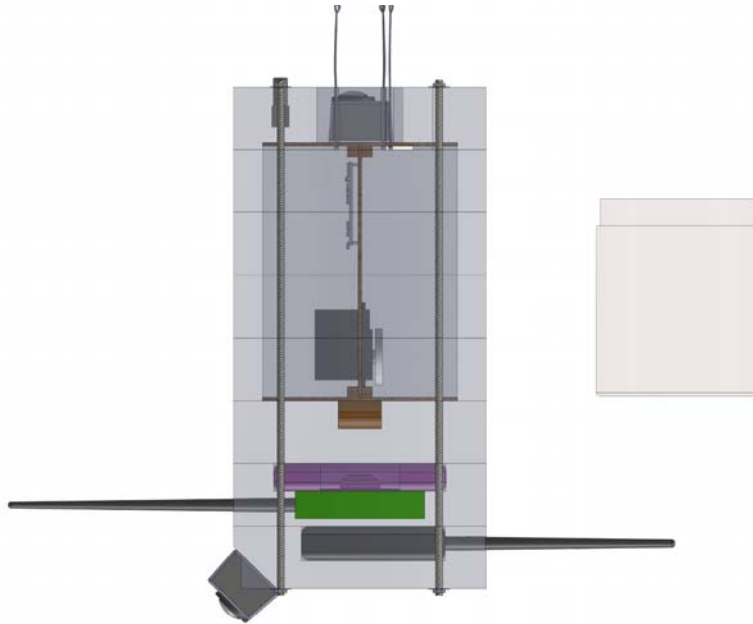


Fig.13. “System A” test system (left) compared to available volume for both the SPQR-ready system and its parafoil stowage (right).

The key driver in the overall size of both Snowflake and System A is the parafoil toggle line tensioning system. This system is necessary to maintain tension on the parafoil steering lines, internal to the payload itself, to prevent the lines from going slack and falling free of the servo spools that control them. If this were to happen, the steering functionality for that servo would be lost entirely, and the added slack in the steering toggle line would also affect the shape of parafoil in its neutral state. This scenario would result in, at best, a greatly diminished, one-directional steering ability, and, at worst, total loss of steering control.

The current tensioning system (Fig.2b) physically requires as large a space for the pulleys to translate as the maximum pulled length of the steering toggle line. That is, if the steering toggle line will be retracted X from its neutral point, the payload-tensioning pulley and spring must also be free to translate that same distance internal to the system. The result of this is a system that cannot be reduced in size beyond the maximum draw length of the steering line. The steering tensioner setup, though quite effective, also adds an undesirable degree of additional

mechanical complexity to the system, with concerns of tensioner line stretching and spring fatigue occurring after long durations of stowage.

The steering control servos are another aspect greatly impacting both volumetric size as well as system total mass. For early development applications (and the scope of this project), control actuator selection is limited to COTS (Commercial Off-The-Shelf) components. Small servos are readily available in enormous variety thanks to the R/C (radio-controlled) hobby industry, but in order to achieve the toggle line deflection required to steer the parafoil without additional mechanical complexity, a special type of servo – a “winch servo” – is required. Unlike standard servos, which rarely have a servo arm travel range of more than 120°, winch servos are geared to provide upwards of three full rotations of their output shaft. These specialized servos are intended for R/C sailboats as a means to actuate their complicated sail riggings. Unfortunately, because R/C sailing is a much less popular hobby than R/C aircraft and cars, the selection of COTS winch servos is very limited. Despite this, there is still room for improvement in System B utilizing COTS servos: the servos currently used by both the Snowflake and System A are roughly twice as large in terms of mass and volume as the smallest available servos with equivalent capability.

As is often the case with payloads intended for space applications, mass of the system must be minimized to the greatest extent possible. This is particularly important for this application, because the heavily insulated, pressurized PCTCU by itself approaches the limits of what can be returned by a parafoil that can be easily packed within its available volume. Parafoil mass is primarily a function of the material used in the parafoil’s construction and the thickness of the shroud lines used. For a given parafoil size requirement, significant mass reduction is difficult without compromising the structural integrity of the parafoil, especially at this scale.

If the parafoil mass is thus assumed to be fixed for a given size of parafoil, then mass reductions must come from the rest of the system. Fortunately, the existing configuration of System A lends itself well to improvement in this regard. The current structure is oversized to accommodate the tensioning system for the steering toggle lines, and therefore mass and volume can be minimized by eliminating the line tensioning system. Also, by simply replacing the servos with smaller, lighter models equivalent in performance, mass will be decreased both in terms of the servos themselves, as well as the reduction of any structure necessary to accommodate them.

The System A architecture provides no means for parafoil deployment (with the exception of the configuration used for the UAV drops, which is not easily adaptable to the SPQR application). In the preliminary balloon flight tests, the entire system has been rigged below the balloon, suspended beneath the collapsed parafoil. Applied to the SPQR system, a highly reliable means of deploying and erecting the parachute must be created. While the deployment system for the parafoil is an element for future development, the effectiveness of adding a semi-rigid structure for improving cell inflation has been demonstrated in the last of the four preliminary tests as described in Section II. It is, of course, not possible to package a set of long carbon fiber stiffening rods into the small volume available for parafoil stowage, so a new means of accomplishing the same outcome must be created. One possible way of achieving this is the use of two small, sealed, flexible tubes which cross the top of the parafoil in the same fashion as the carbon fiber structure. These tubes would then meet in the center of the parafoil, and merge into a single tube that travels along one of the parafoil’s shroud lines to the deployment canister. Upon deployment, a miniature CO₂ cartridge would be punctured and inflate the small network of tubing, thus providing a degree of rigidization from the internal pressure within the tubing. Development of this concept would include tests of tubing of different material composition and varying diameter to evaluate their structural rigidity upon inflation, and the ability of the tubing material to be folded and tightly packed for long durations without kinking and sealing internally when deployed.

In addition to the deployable parafoil, there must also exist a means of deploying the GPS antenna of the guidance system above the interior volume of the parachute stowage compartment. If this is not done, the viewing field of the antenna will be greatly obscured by the walls of the PCTCU parafoil compartment, and unacceptable GPS signal attenuation will occur. This consideration is another item of future development, but a simple proposed solution is the attachment of an omni-directional helix antenna to a low point on one of the parafoil shroud lines, which would deploy the antenna with the parafoil upon release.

Typically in space flight applications, one of the more significant challenges of system design is the unforgiving thermal and vacuum environment. Many design-simplifying characteristics that we take for granted on Earth, such as natural convection for heat dissipation, and a moderate thermal environment where ambient temperature and incident radiation vary minimally, do not exist in space. Instead, an orbiting satellite is subjected to extremes of heating and cooling, often with one side exposed to unfiltered solar radiation while the other radiates to the near-absolute-zero abyss of deep space.

The lack of atmospheric pressure also poses some surprising challenges: many of the common materials we use on Earth have very undesirable outgassing properties when placed in vacuum, sometimes resulting in compromised material properties or damage to sensors or optics of the spacecraft.

Fortunately, the parafoil system for use in SPQR has the luxury of a benign, Earth-like thermal environment from launch to return. This is the result of its being stored in the PCTCU, which is a passively thermal-controlled container, designed to accommodate the strict thermal requirements of biological samples upon return from the ISS. Also, prior to deorbit and reentry, the entire SPQR system is intended to be stored internally in the ISS - a very Earth-like environment, gravity excluded.

The parafoil steering assembly will, however, be subjected to a vacuum environment during deorbit (and possibly transport to the ISS), so careful attention must be placed on materials selection to prevent any issues that may arise from this. Certain plastics are thus eliminated from consideration, and any necessary internal lubrication (*e.g.* the internal servo gears) must be done by a vacuum-rated grease or dry lubricant. Most common greases for planetary applications undergo significant, detrimental property changes after being subjected to near-vacuum conditions.

In addition to all the above complexities, any device that is to be taken to the ISS or placed onboard the ISS is held to an enormity of further constraints, intended to guarantee the safety of the ISS and its crew. Applied specifically to the parafoil subsystem of SPQR, the key constraints are battery selection, redundancy of activation systems, stored energy requirements (which may be applicable to parafoil deployment), and materials outgassing. It is beyond the scope of this project to address these to the extent necessary for space flight approval, but an awareness of these constraints while designing the System B test article will prevent design decisions from being made that cannot be easily transformed into a space-certified system.

B. Mechanical Design of a PCTCU-Compatible Unit

Based on the design criteria outlined above, a new mechanical architecture for the parafoil steering system has been designed, as shown in Figs.14 and 15. Improvements to the old System A architecture have been made in terms of size, mass, mechanical complexity, strength, and packaging efficiency. The GNC unit for the new design (System B) is only 13.8cm (5.44”) in diameter and 4.86cm (1.9”) tall.

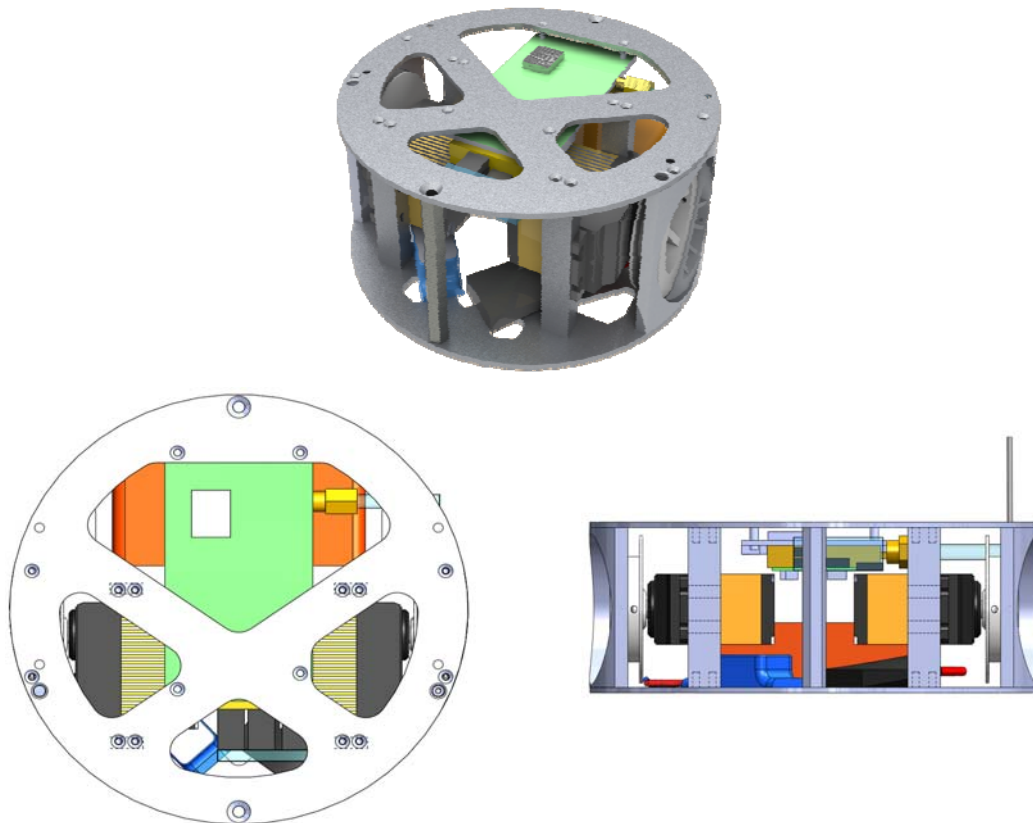


Fig. 14. Miniaturized GNC unit.

Figure 16 shows the old architecture compared to the new system to indicate a sense of scale. The new system is volumetrically compatible with the PCTCU containment volume, while still maintaining the majority of the

compartment's volume for parafoil stowage and deployment systems. Regard has been given to minimizing the mechanical complexity of the system, keeping fabrication as simple as possible, and maintaining high reliability within the mechanical steering system. The transparent red cylinder around System B in Fig.16 indicates the remaining available payload volume for parafoil stowage and deployment systems.

Significant reduction in size was achieved through several means: minimizing empty space in the device; selection of smaller servos while maintaining equivalent performance capability; converting structures to a horizontal stacked deck configuration instead of the previous, volumetrically-inefficient vertical deck; and the complete elimination of the pulley tensioning system.

Table 1 gives a component breakdown of total system mass for both the old and new system architecture. The primary mass savings are gained through selection of new servos, and less inert structural mass (which included the pulley tensioning system and all associated hardware in the old design). These improvements have resulted in a considerable 87% reduction in system volume, and a 39% reduction in overall system mass for the parafoil steering system mechanics.

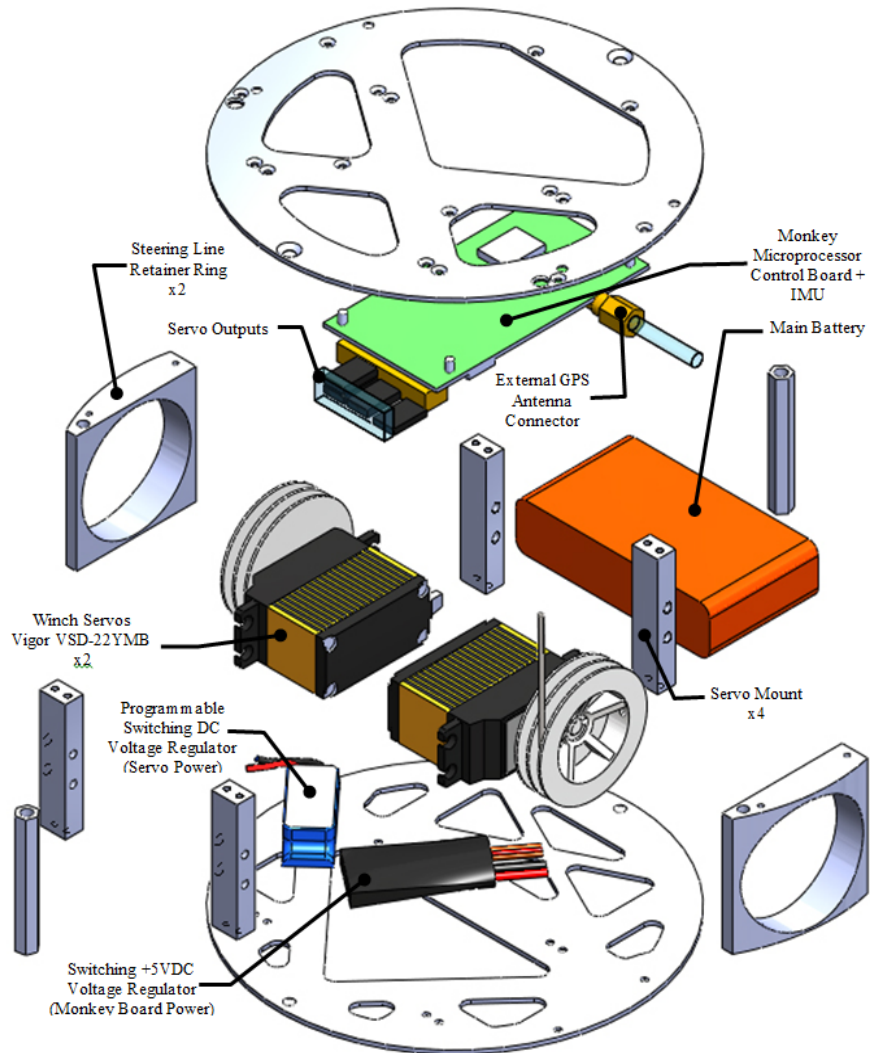


Fig. 15. Exploded view of a new design.

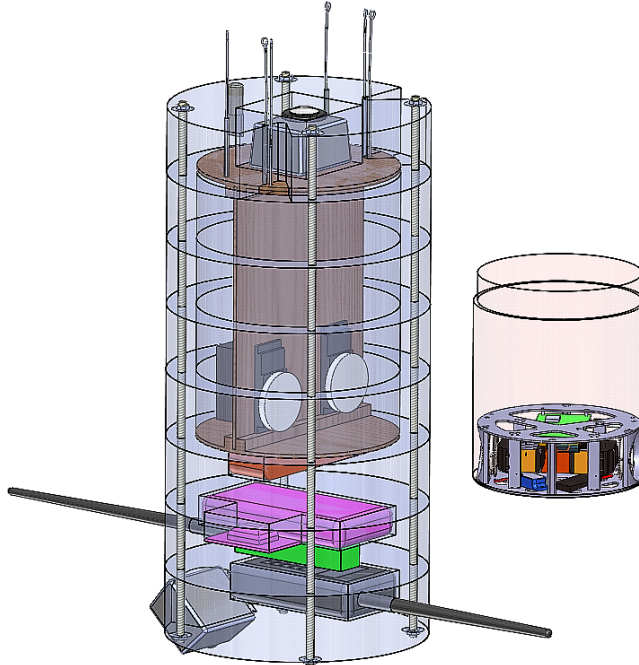


Fig. 16. Side-by-side comparison of two designs (Systems A and B).

Table 1. Mass and power breakdown for components of System A and B.

	Component	Qty.	Mass Each (g)	Mass Total (g)	Input Voltage (V)	Ave. Current Draw (A)	Max. Current Draw (A)	Ave. Power Usage (W)	Max. Power Usage (W)
System B Config. (New)	Battery	1	241	241.0					
	Servo + Wheel, VSD-22YMB	2	56	112.0	7.2	0.3	3	2.16	21.6
	Structural Assy. (no fasteners)	1	55.42	55.4					
	Monkey2010 + Chimu	1	33.5	33.5	5	0.15	0.18	0.75	0.9
	GPS antenna + full cable	1	30	30.0					
	2 port 5V VR + Servo Wire	1	16	16.0	7.4	0.01	0.01	0.074	0.074
	CastleBEC Voltage Regulator	1	15.5	15.5	7.4	0.01	0.01	0.074	0.074
	Fastener Margin (10% Structure)	1	5.542	5.5					
Column Totals:				509.0		0.47	3.2	3.058	22.648
System A Config. (Old)	Structural Assy.	1	267	274.0					
	Battery	1	241	241.0					
	Servo + wheel, HS-785HB	2	110	220.0	4.8	0.23	3	1.104	14.4
	Monkey2010 + Chimu	1	33.5	33.5	5	0.15	0.18	0.75	0.9
	GPS antenna + full cable	1	30	30.0					
	2 port 5V VR + Servo Wire	1	16	16.0	7.4	0.01	0.01	0.074	0.074
	CastleBEC Voltage Regulator	1	15.5	15.5	7.4	0.01	0.01	0.074	0.074
	Column Totals:				830.0		0.4	3.2	2.002

To significantly reduce the size of the old system, a new means for maintaining pulley line tension had to be devised. The old system, while very effective and quite reliable, increased system mass, overall complexity, and prevented the dimension along the axis of control line actuation from being smaller than the maximum control line pull distance. The new system utilizes a much simpler, extremely reliable, passive approach to accomplishing the same end goal of the previous tensioner rigging. By surrounding the servo wheel with a precise, close-fitting ring, the steering toggle line is held captive in the servo wheel groove, preventing it from falling free regardless of line

tension. The captive ring has a hole located precisely above the servo wheel where the line must exit to the parafoil (Fig.17). In this arrangement, regardless of line tension, it is not possible for the line to fall completely free of the servo wheel, and any slack in the line will quickly be taken up upon parafoil inflation (assuming appropriately sized lines are used). The servo wheel containment ring doubles as a structural support member in the steering assembly stack. This solution to the tensioning problem is deceptively simple, but when extremely high reliability is desired in space applications, a simple, passively self-working design often has far fewer failure modes than a complex mechanism. For example, by eliminating the volumetrically inefficient, mechanically complex pulley tensioning system and springs, the new design has also addressed any concerns of spring aging and weakening, special lubricants required at friction points of the pulley wheels, potential for tensioning lines to vibrate free of their pulleys under launch loads, and possible resonance associated with the spring system.

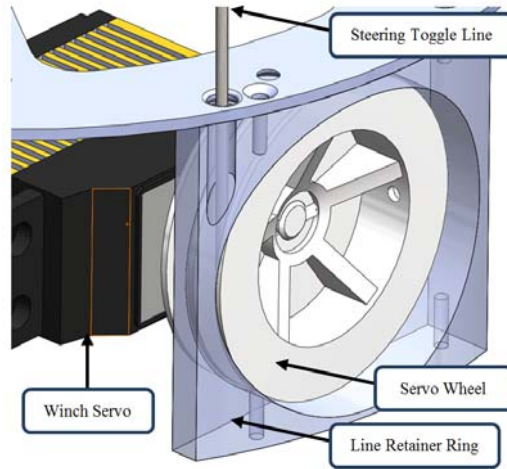


Fig. 17. Detail of the structural ring (shown transparent) used to keep the steering toggle line captive in the servo wheel.

To ensure reliable functioning of the captive ring system, proper selection of the line to be used is crucial. Lines should be as small in diameter as possible, without being so small that they could become pinched by the 0.010” clearance between the servo wheel and the containment ring. Lines that are too thick could potentially double over in the servo wheel groove and cause a temporary bind to occur. Experimentation was carried out with a large variety of line types and sizes, from braided nylon, to monofilament fishing line, to very lightweight plastic weed trimmer line, in order to identify the potential failure mechanisms of the captive line design. Based on these tests, it was found that a very flexible line with a diameter just greater than the clearance between the servo wheel and containment ring was ideal for reliable operation and to prevent any internal binding. For flight testing of System B, a braided 0.030” (0.76 mm) diameter nylon cord was used with great success.

To determine servo requirements for component selection, servo torque, operating voltage, current draw, size, mass, and transit speed (the rate of output shaft rotation) must be considered. Using the existing servos in Snowflake and System A as a baseline, a search of available COTS winch servos was carried out. Due to the very limited demand for winch servos in small applications, the options are quite limited. Table 2 presents the available COTS winch servos found and their individual specifications.

Table 2. Commercially-available winch servos in the size range of interest.

Servo Model	Mass (g)	Dimensions, LxWxH (mm)	Operating Voltage Range (V)	60° Transit Time (s)	Stall Torque (N-cm/9.81)	Max. Rotation Angle (Deg.)	Drum Diameter (mm)	Digital / Analog	Gear Material
Futaba S5801*	83	46x23x44	6.0 - 7.2	0.10 - 0.08	7.8 - 9.8	1980	30	Analog	Metal
Hitec HS-785B	110	59x29x50	4.8 - 6.0	0.28 - 0.23	11.0 - 13.2	1260	37	Analog	Karbonite
Graupner Regatta	90	46x41.9x23.1	4.8 - 7.2	0.17 - 0.11	5.4 - 10.2	1980	38	Analog	Nylon
Graupner Regatta Eco	70	46x41.9x23.1	4.8 - 7.2	0.2 @ 6V	4.5 @ 6V	1980	38	Analog	Nylon
Vigor VSD-22YMB	56	40.6x20x38.9	6.0 - 7.2	0.12 - 0.10	9.5 - 11	2160	30	Digital	Metal
GWS S125 3T	50	40.5x20x42	4.8 - 6.0	0.26 - 0.21	9.2 - 10.2	1080	30	Digital	Nylon

*Servos used in original Snowflake configuration

Using data logs from the flight tests of System A, accelerations measured by an on-board inertial measurements unit (IMU) gave precise numbers for typical loadings seen throughout flight. Some of the data represents nominal flight conditions, while other data points were obtained in violent, high-angular-velocity tumbles with a collapsed parafoil. Specifically, a peak on-axis acceleration measured by the IMU during a UAV flight test (where the parafoil was deployed at a velocity of approximately 50mph (22m/s)) was at deployment at 48.6m/s^2 , *i.e.* 4.95G, while for a gentle balloon release with a pre-deployed parafoil it was four times less, 12.64m/s^2 , *i.e.* 1.24G. Using these data, bounds (with a reasonable design margin) were placed on expected acceleration loads in both normal flight as well as maximum stressing conditions.

Assuming that the descending parafoil and payload is very nearly in static equilibrium, Newton's Second Law allows computation of the total force exerted on the shroud lines to suspend the payload. Dividing the total force by six gives the approximate static loading on each individual servo, assuming that the payload mass is suspended equally by the four suspension line groups and the two steering line groups. (This is a highly conservative design estimate, because in reality the majority of the payload weight is carried by the suspension lines and not the steering toggle lines.) Finally, the static load per servo is converted to the torque applied to the servo output shaft by multiplying the force by the servo wheel radius. Obviously, the aforementioned approach leads to quite conservative estimates of the static loading. Excluding the stages of parafoil deployment and sharp turns the actual loads are likely to be of an order of magnitude less.

The servo transit speed also plays an important role in system performance, but the associated requirement is more difficult to quantify. In essence, the servo must respond quickly enough to command inputs to initiate a turn without creating such a lag in response time that the guidance algorithm cannot properly compensate. A faster servo will be beneficial for greater turning authority in flight and in final landing corrections. To complicate matters, the parafoil-payload system also has an inherent control latency of its own. When the steering toggle line is first pulled, there is a slight delay between the deformation of the parafoil and the actual initiation of the turn. The parafoil then begins its turn, but the non-rigid connection to the payload through the shroud lines causes a delayed rotation of the payload as the lines twist and then unload. Depending on the attitude determination scheme used, this can be more or less of a problem. For example, a magnetometer serving as a compass will sense only the orientation of the suspended payload, so it will not "see" a response to a commanded turn until the twisting of the shroud lines overcomes the rotational inertia of the payload, causing it to turn as well. Alternatively, a GPS-based attitude determination will calculate heading based on translation of the payload rather than magnetic field alignment, so the flight control algorithm will be blind to any twisting of the payload beneath the parafoil.

The diameter of the servo wheel factors directly into the servo transit time, because a larger wheel will pull more line for a given angular displacement, but requires greater torque to do so. Using the original servos utilized in the Snowflake system as a baseline, the servo transit times and wheel diameters are presented in Table 2 for the different servos considered. Because the servos all have similarly sized wheels, it can be assumed that any servo with an equivalent transit time to the baseline servo will perform acceptably in this application, because the Snowflake steering algorithm has already been proven effective at this response rate.

The final key considerations in servo selection are operating voltage and power consumption (to be addressed later in this section). Based on all of the above, the Vigor VSD-22YMB servos were chosen due to their small size, comparatively light weight, high torque, acceptable power consumption, metal gear train, and impressive transit speed.

The structural components of System B have been kept as simple and minimal as possible. The entire structural assembly consists of only ten major parts total, and of these ten parts, only four are unique. With a mass of only 55g, the structural assembly provides the backbone that supports all the components of the steering system while contributing minimal weight. The design utilizes two circular discs of 0.063" (1.6mm) aluminum, which are joined together at eight points distributed across their faces. The structure is extremely strong and rigid, and more than adequate for supporting the weight of the PCTCU system beneath the parafoil. The complete, assembled System B hardware as tested is shown in Fig.18.

C. Electronics System Design

As shown in Fig.15, the electronics system for the parafoil steering system has very few individual components, consisting of the main battery, two DC voltage regulators (one for processor board power and one for dedicated servo power), a control system microprocessor board, and two servos (Fig.19). A distinction should be made at this point between the System B design (as presented in this work) versus a flight-ready, space-worthy electronics system. For the former, a multi-function microprocessor board with an integrated IMU provides the complete system intelligence, but in actuality some aspects of the board's capabilities are overkill for this application, and an even smaller custom system could be designed with more specialized electronics. For a spaceflight-ready design, the

electronics systems and software algorithms would have to undergo very rigorous testing to guarantee reliability and performance. Also, if smaller electronics boards were implemented, redundant processing systems could be utilized to ensure a greater degree of reliability.

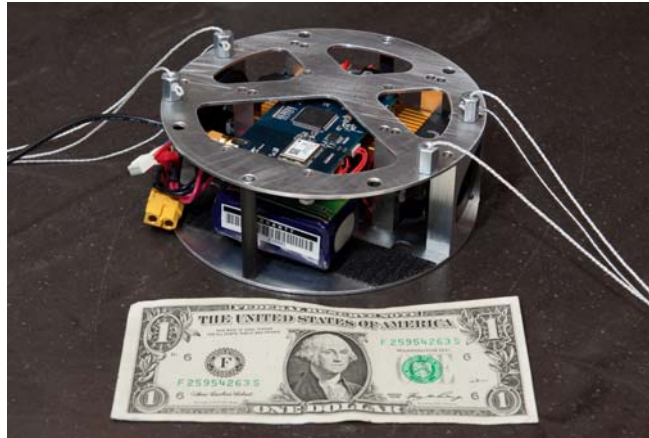


Fig. 18. The complete System B control hardware after fabrication and assembly.

The programmable microprocessor board (a Ryan Mechatronics Monkey Cortex navigation platform) utilized for this design iteration provides an extremely capable, flexible, all-in-one solution to attitude determination, 3-axis rate sensing, and 3-axis acceleration measurements (via the on-board IMU), software execution, spatial position determination (via GPS), and pulse-width modulation (PWM) servo commanding. Also, built-in data logging to a microSD card records all flight parameters at 10Hz, yielding a complete time- and location-stamped set of system performance data for each flight test. (The latest version of the Monkey autopilot, X-Monkey, has more functionality and is roughly half the size of the 2010 version.)

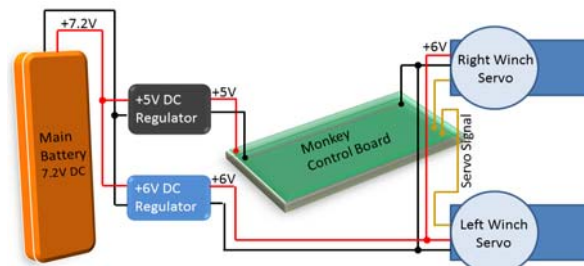


Fig. 19. Electrical block diagram for the parafoil steering system.

Given the fairly simple electrical design of the system, there is little to be done beyond individual component selection. Two key areas that require extra attention are battery selection and power distribution. The battery is the heaviest individual component of the entire steering system, so it is important to choose a battery with sufficient capacity to power the entirety of the flight (with appropriate design margin) without adding extra “dead weight” to the system. Also, the nominal voltage of the battery must be greater than the required input voltage of any of the individual components, because the switching-mode voltage regulators chosen for System B cannot increase voltage beyond the battery input voltage. For a given battery chemistry, pack voltage is determined by the number of cells in series in the battery pack.

With the power consumption of all components shown in Table 1, the estimate of the required battery capacity is based on the knowledge of a typical duty cycle for the servos. First, the descent time is estimated based on the descent rate (as discussed in Section III). Then, time histories of the instances of servo actuation for a nominal flight (estimated at low-altitude drops from a UAV and extrapolated to the high-altitude deployment) allow computing duty cycles for the servos.

As previously noted, the integrated System B design presented in this paper is not a space qualified system, but the additional factors required to make it spaceflight-worthy have been taken into consideration at each step. Compared to the other subsystems, the electrical system as-presented would require the greatest degree of modification and additional testing to be approved for ISS safety. This can be minimized through an awareness of these factors during preliminary design.

A primary concern for bringing payloads aboard the ISS is battery chemistry selection and battery pack design. Only certain battery chemistries are approved for use, and of those chemistries, the individual cells must have appropriate safeguards installed as well. This includes venting in case of battery overpressure (e.g. from a cell overheating), and protective diodes installed to prevent reverse current flow into each cell. The process of getting a newly-developed battery pack approved for ISS use can be time-consuming, rigorous, and expensive, but can be circumvented if the system utilizes batteries that have already been approved for prior missions.

The operational duration of the parafoil system for ISS payload return and the preliminary System A balloon tests will differ very little in terms of total time powered-on and time to payload recovery. Both the full-fledged SPQR system and the System A balloon-test platform begin their mission phases at comparable altitudes, and the actual ISS return scenario will have greater resources focused on payload trajectory, tracking and recovery than an amateur balloon test. For these reasons, it is reasonable to expect that total power requirements for System B and the actual SPQR parafoil return system will be similar, and the battery's mass and volume accommodations will be compatible for both (assuming the SPQR device has an independent battery for the parafoil system, which has yet to be defined in the larger SPQR concept).

Another consideration that poses great difficulty on-board the ISS is battery charging - for most applications, especially ones intended to be as simple as SPQR, charging onboard the ISS should be avoided. For the parafoil return system (and indeed the entire SPQR system), primary (non-rechargeable) cells are preferable for several reasons: the approval process for ISS use is greatly simplified if charging is not required; primary cells have a much lower rate of self-discharge in storage compared to rechargeable cells; primary cells offer excellent energy density; electronics system design is simplified without including a charging circuit; solar cells for space applications add significant cost; and, the short operational duration and modest power consumption of the SPQR and parafoil systems pose no need for in-flight solar recharging.

If any of the electronics of the parafoil system were in a powered-on state aboard the ISS, extensive testing of the electrical components and control board would be required to satisfy safety requirements. However, if the electrical systems can be guaranteed to be completely isolated from battery power at any time prior to release from the ISS, this safety concern is eliminated. For this reason, the parafoil system will utilize redundant activation switches in series with the battery, thus requiring both of the switches to be closed before the electronics of the parafoil system will be powered-on. One of the switches will be activated by removal of a remove-before-flight pin (common in such applications) prior to the jettison of the SPQR system from the ISS, and the second switch will be activated just prior to reentry, when the reentry vehicle is separated from the SPQR de-orbit system.

Other common spaceflight concerns for electronics include radiation hardening, thermal and vacuum environments, and tolerance to shock and vibrational loads. The short lifetime in-orbit (on the order of several days), combined with the containment inside the PCTCU structure negates the need for radiation hardened components, particularly if redundant processing boards are utilized. The systems must undergo thermal vacuum testing for space-worthiness, and shock and vibration testing as well. The shock and vibrational loads encountered by the system in actual use are likely to be very modest, because the SPQR device would likely be carried as a "soft-stow" item aboard an ISS resupply vehicle.

V. Testing Control Algorithms

With so many other challenges for the high-altitude drops, System B utilized a somewhat simplified guidance paradigm (compared to that of Snowflake⁷) that is supposed to guide the system directly and precisely to a target set of latitude/longitude coordinates upon release (Fig.20). After arriving above the target point, at any altitude, a simplified guidance dictates to fly a controlled spiral pattern to the ground.

To ready the software for a flight to a specific target (programmed in C), only three main parameters must be entered: target latitude, target longitude, and target altitude. After these parameters are input, the software routines handle the rest of the control necessary to guide the device to the target and land. There are a number of other various inputs to the control scheme which are "tuning parameters" - they have a significant effect on the steering performance, but once appropriate values have been selected, they should not need to be changed often.

The guidance algorithm is based on a single main control loop, which runs at a rate of 10Hz. When the control loops is initiated, it immediately queries the Monkey board's GPS chip for current latitude, longitude, and altitude. These are updated by the GPS at a rate of 4Hz, typically. The latitude and longitude are passed as inputs to a form of the haversine formula, re-cast to work with the standard math library of the C coding language. The control algorithm computes the magnitude of the great-circle distance from the parafoil system's current location to the target coordinates in meters and the heading (0 to 360°).

While the detailed discussion of the control algorithm is beyond the scope of the current paper (some details on the simplified algorithm can be found in Ref.[12]) here are some of the specifics not dealt with by other parafoil

guided systems before: zero-speed deployment, very different dynamics at different altitudes (changes in air density along with varying added mass coefficients affect damping properties and canopy-payload interactions), layers of strong steady winds (both head- and crosswinds), necessity to carry out computations in the Earth-centered inertial coordinate frame (operations start at 20-30km above the surface of the Earth and the descent lasts tens of minutes or even more than an hour).

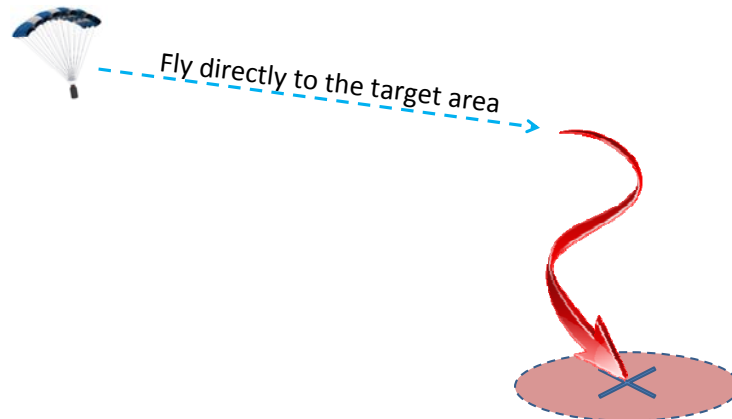


Fig. 20. Pictorial concept of operations for System B flight software control scheme.

The proposed parafoil stiffening structure (Fig.8) mitigates the effect of a zero-speed deployment and low air densities, and the gain scheduling should be implemented to account for changing dynamics at varying atmospheric density throughout descent. As far as the strong winds aloft the success of the mission obviously relies on a good knowledge of them to calculate a reachability set and build the best guidance strategy. Figure 21a features one of the typical wind profiles as collected by the weather balloon (it actually shows the so-called ballistic winds computed as discussed in Ref.[13]). As seen, not only do they change magnitude and direction depending on the current altitude, but for the most part they are quite strong, well exceeding the forward speed of a miniature payload return system. In a strong headwind, the parafoil system may remain stationary relative to a set of coordinates, or actually fly backwards relative to a fixed point on the ground, despite facing directly into the wind. In this scenario, it may be impossible for the parafoil system to ever reach the target even under perfect control. As shown in Fig.22b, if the parafoil is directly downwind of the target, and the wind velocity is exactly equal to the forward glide velocity of the parafoil, the actual range of vectors the parafoil is capable of flying is limited to a direction away from the target. As the wind velocity becomes greater than the glide velocity, this vector distribution becomes increasingly narrow in width and more elongated in the direction of the wind vector.

To verify the performance of the many iterations of the steering routine written for this work, three levels of testing were used. For initial code performance assessment, and to eliminate any obvious functionality bugs, the software was first compiled to run on a Windows-based computer, and a large set of fictitious flight data was supplied to the flight algorithm. Compiling the software and testing it in this fashion takes less than a minute, so this method was used regularly throughout the software writing process to ensure obvious logic errors were caught prior to flight testing.

After completing an iteration of the software code and performing initial validation on the PC, the code was then compiled for the ARM-based microprocessor of the Monkey board and the software written to its flash memory. A series of hardware-in-the-loop simulations took place. Upon power-up, a servo test routine runs first, which moves the servos to maximum, minimum, and neutral toggle line extension positions. Then, the board attempts to get a 3D position fix from the GPS, and once this occurs, the steering processes become noticeably active. A quick assessment that can be performed at this stage is to set the target coordinate to some nearby location and walk with the device outdoors to see if the servos respond in generally the correct direction relative to the direction of movement.

The next step in testing algorithms was to employ an electric radio-controlled helicopter, capable of lifting approximately 3lbs (1.36kg) (Fig.22). It was modified to allow attachment of a tether line to the parafoil system. The helicopter was then used to lift the entire parafoil system, including an on-board video camera, to an average altitude of 80m above a steep hill, and the system with the pre-deployed canopy was then released via a switch on the controlling transmitter. The helicopter lifting the parafoil with the tether setup is shown in Fig.23a. Utilizing the helicopter in this fashion allowed for multiple drop tests (over 40 drops in total) to be conducted in a fairly short

interval, with average descent times of 20-30 seconds, depending on winds and steering system performance (Fig.23b).

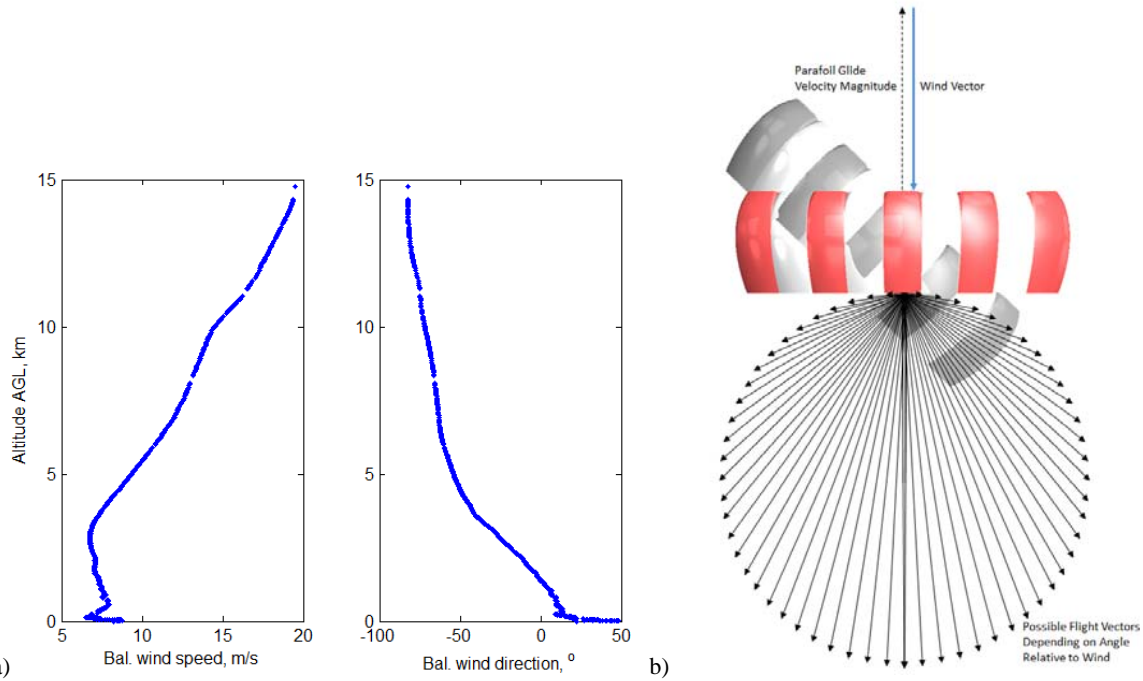


Fig. 21. Example of the ballistic winds versus altitude (a); range of possible flight vectors when wind velocity is exactly equal to parafoil glide velocity (b).



Fig. 22. R/C helicopter used for lifting System B.

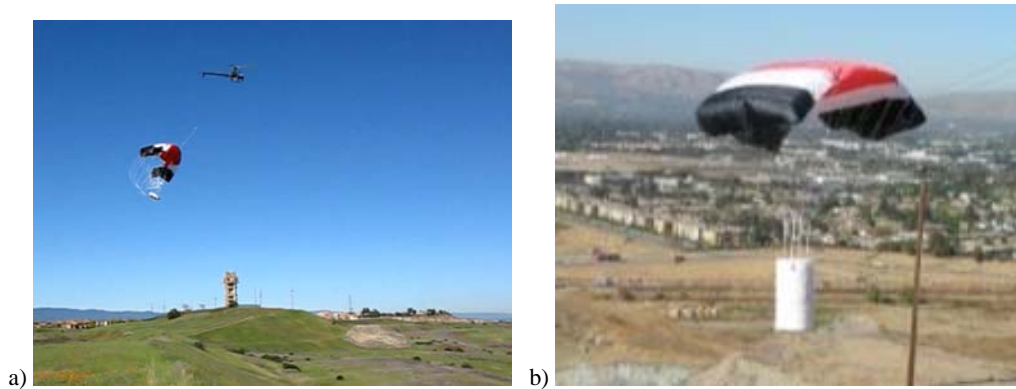


Fig. 23. Video capture of parafoil being lifted by the R/C helicopter (a); System B in flight (b).

Following the series of helicopter drop tests for control refinement, a final set of higher-altitude drop tests were conducted from a UAV at altitudes of 1,500-2,000ft (457-610m) AGL. These tests demonstrated the ability of the control software to manage flight over a much greater distance and for longer descent durations. For these tests, both System A and System B were programmed with the newest versions of the flight software, and flight data was logged for each system to generate as much performance data as possible. The steering systems as configured for the UAV drops are shown in Fig.24a, and the payloads mounted on the Arcturus T-20 UAV are shown in Fig.24b. Figure 25 shows the ground target as captured by onboard camera, while Fig. 26 captures a moment right before touchdown.

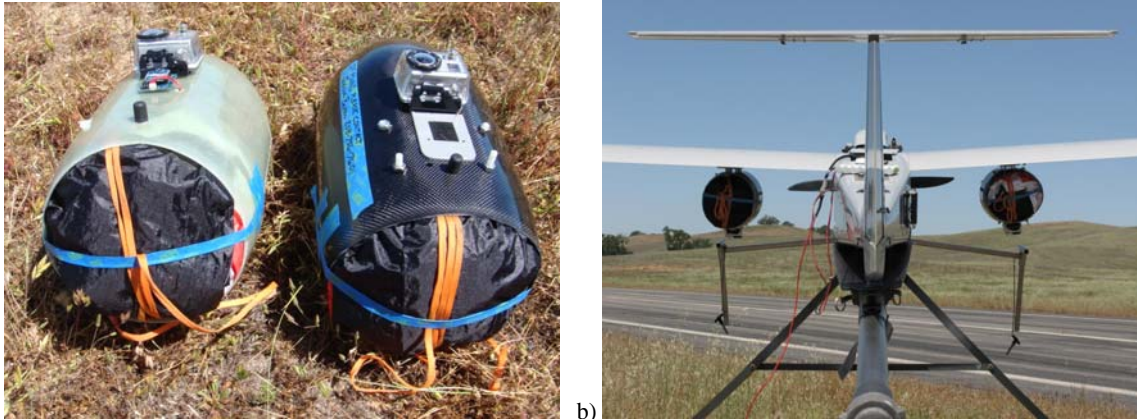


Fig. 24. System A (left) and System B (right) as configured for the UAV drop tests (a); both systems are ready to go (b).



Fig. 25. Video capture from System B as it steers towards the target, located approximately midway down the runway.



Fig. 26. System A arriving near the target point on the runway.

Figure 27 shows a compilation of distance-to-a-target time histories for several helicopter and one UAV drops featuring different dynamics of the system due to various control gains.

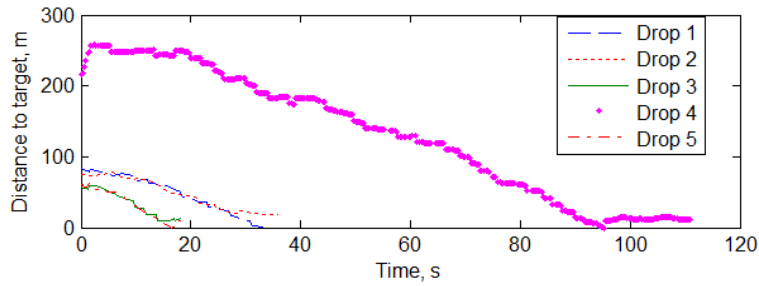


Fig. 27. Time histories of two-dimensional distance to the target while varying controller gains.

VI. High Altitude Balloon Drops of SPQR-Ready System

As discussed in the previous section, test planning heavily relies on Winds Aloft Forecasts provided by the Centers for Environmental Prediction (<http://rucsoundings.noaa.gov/gifs/>). Based on these predictions the VAST team computes the balloon release point. For the purpose of constructing a reachability set to the SPQR payload delivery system and assigning a feasible target the Safety Fan GUI¹³ developed for the Yuma Proving Ground earlier is employed (Fig.28).

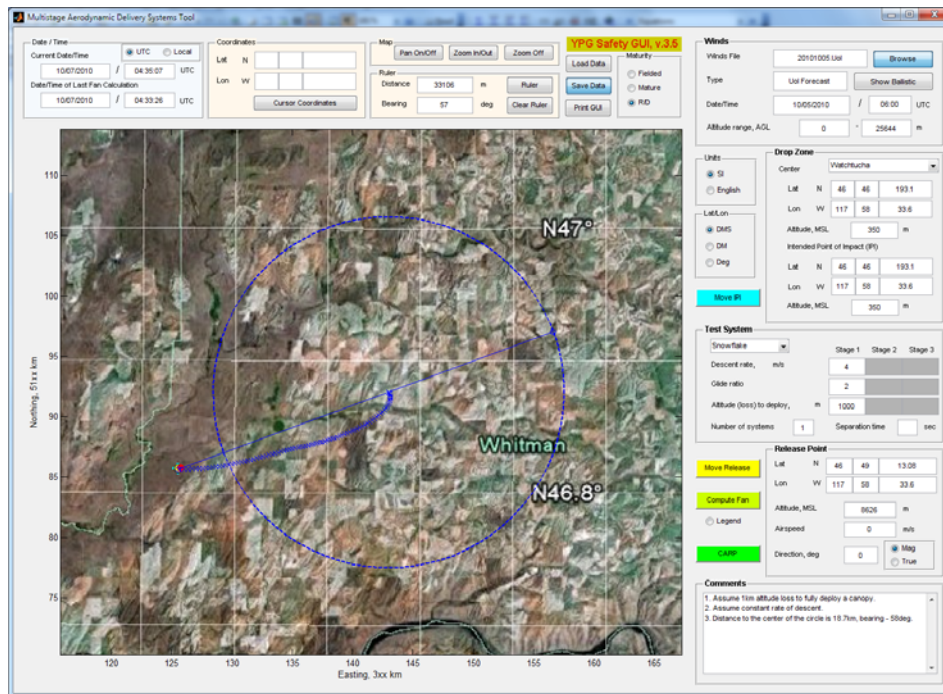


Fig. 28. The YPG's Safety fans GUI employed for the low-stratosphere drops.

The first high-altitude flight test of the system B was conducted in Northern Idaho on May 19, 2012 (Fig.29). The system utilized the semi-rigidizing parafoil structure, and cutdown from the balloon was commanded from 50,000ft (15,240m) altitude via a new Iridium satellite-based control module developed by the University of Idaho. The cutdown was a complete success, occurring precisely at the desired altitude, and the parafoil system was released without incident (Fig.30).



Fig. 29. The parafoil system carried away on the balloon shortly after launch (a); downward view from the fish-eye camera from another payload above System B (b).

Immediately upon release, the parafoil began a brief spiral until its line tensioner attachments (used to prevent snags on ascent) were jettisoned. The parafoil then quickly settled into a highly stable flight path (Fig.31), still well above 49,000ft (14,935m) altitude, and gliding with the wind at a groundspeed of 12m/s (39ft/s). As the parafoil descended, the groundspeed varied between 5m/s (16ft/s) and 33m/s (108ft/s), dependent on the strength of the prevailing winds at different altitudes.



Fig. 30. View from the up-looking camera after successful parafoil inflation at 50,000ft altitude ASL.



Fig. 31. The parafoil system cutdown.

Unfortunately, the parafoil system's control board shut down prior to cut-away from the balloon. The exact cause of this failure is still unknown, but it is believed to be the result of a new battery used with much greater sensitivity to cold temperatures than the battery used in previous flight tests. Because of this control board power failure, the parafoil descended in a glide with the wind throughout nearly its entire descent. Just a few minutes prior to landing, the control board re-booted and steering resumed. Though the system immediately corrected its heading

toward the predefined landing target, this occurred with only a few thousand feet of remaining altitude. Though the shutdown of the control system was disappointing, its root cause is thought to be easily corrected for future flight tests, and the successful inflation and highly stable flight of the miniature parafoil at 50,000ft altitude ASL was a very exciting development.

Two more drops were carried out in 2012 (on 8/17/12 and 9/29/12). Figure 32 demonstrates a typical altitude profile as recorded by APRS within System B and the rest of the balloon train. After releasing System B, the balloon continues to ascend until it bursts. The remains of the system (with other balloon train payloads) are being carried down by a round parachute. Figure 33 features a time history of the vertical speed of System B corresponding to data of Fig.32. Figures 34 and 35a represent the ascent/descent profiles for the balloon and System B for the same drop.

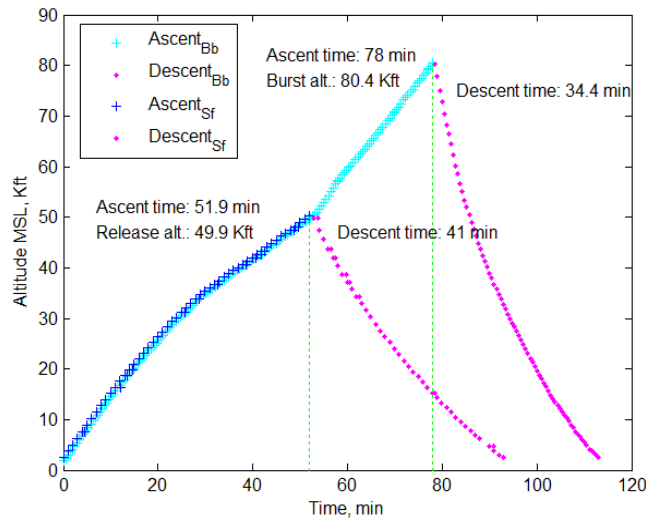


Fig. 32. Time histories of the altitudes for the balloon and System B.

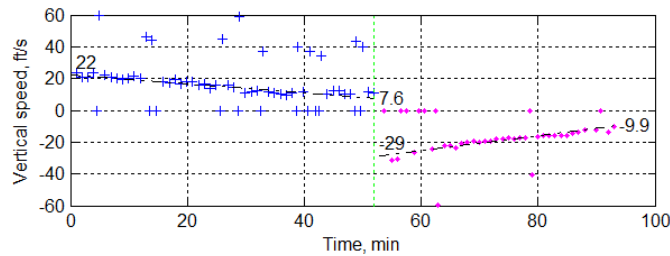


Fig. 33. Time histories of the vertical speed for System B.

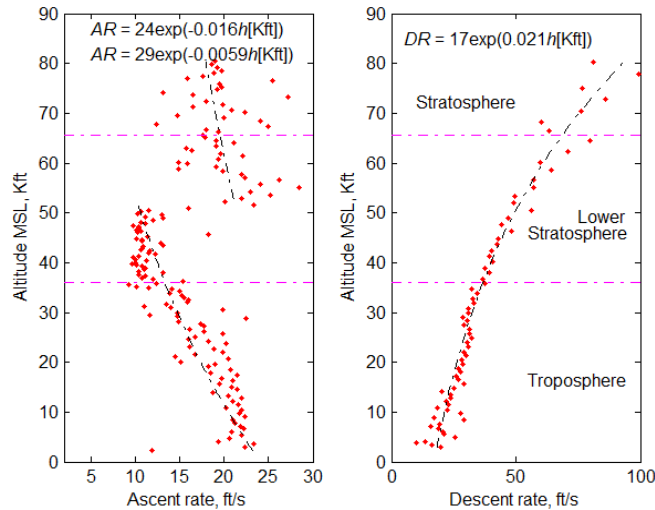


Fig. 34. Vertical speed versus altitude for a balloon.

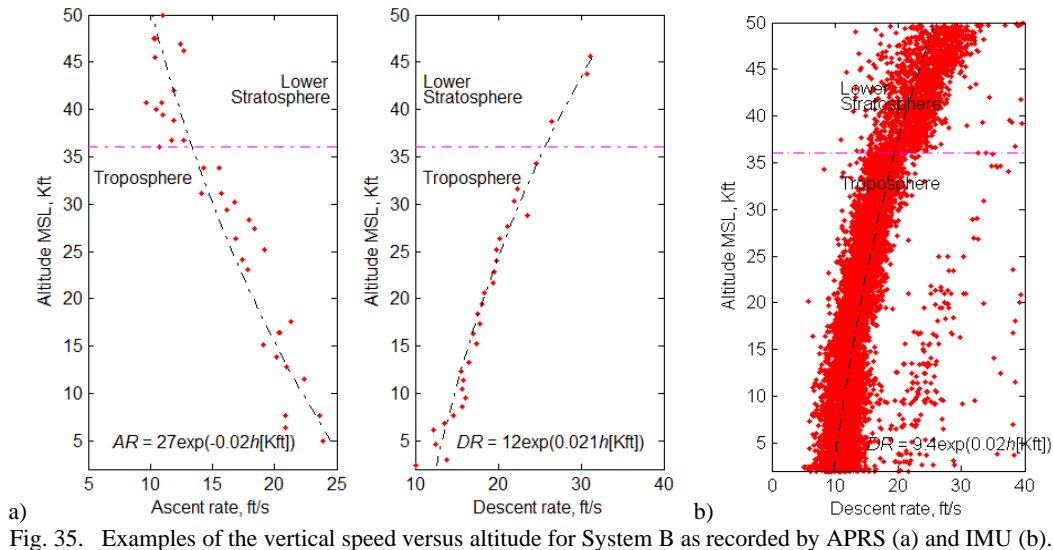


Figure 35b shows an example of GPS data for System B, for another drop. As seen, the regression curves for a descent rate in Fig.35 coincide with that of Fig.11 and therefore the actual descent time is very close to that predicted by Eq.(12).

Since there is a limit of having only three low-stratosphere drops per year to occur within May-September frame to avoid strong eastward moving jet streams over Washington and Idaho states, further experiments are expected to be carried in summer of 2013.

VII. Acknowledgments

The authors would like to thank Marcus Murbach of NASA Ames Research Center for introducing them to the SPQR concept, CDR Chas Hewgley for assisting in building System A, and the crew of Arcturus UAV for providing a capability to do the low-altitude drops from their highly-advanced UAS. Special thanks and recognition goes to Dr. David Atkinson, Kevin Ramus and the entire University of Idaho VAST team (Fig. 36) for providing the launch opportunities to test the SPQR parafoil system from very high altitudes beneath their balloons.



Fig. 36. The authors with the University of Idaho VAST team.

VIII. Conclusion

The paper presented the current status of the development of a small autonomous parafoil system compatible in size, shape, mass, and general operation with the ISS on-demand sample return concept SPQR. The parafoil system has been optimized with regard to structural efficiency, and has simultaneously incorporated design refinements that reduce complexity, improve reliability, and minimize potential failure modes. Custom control software for the parafoil system has proven effective in a range of flight tests, demonstrating a consistent ability to guide the device to a predefined set of target coordinates, even in the presence of moderate crosswinds. In addition, the parafoil system has been designed with its intended application to spaceflight payloads in mind, reducing the extent of future design revision required to bring the device to a spaceflight-ready level of development. While primarily intended to fill the role of a terminal descent recovery device for SPQR, many other attractive applications of the technology exist at a range of scales, from payload return for amateur high-altitude balloon experiments, to the targeted delivery of sub-orbital sounding rocket payloads. Future work for the parafoil system as a whole, applied to SPQR, includes further tuning of the control algorithms along with the development of both the parafoil deployment system, and a compact, deployable means to assist the parafoil with rapid inflation at high altitudes. An inflatable variant of the carbon-fiber cross structure presented in this paper may provide the solution to the latter, and the compact design of System B ensures feasibility of the former.

References

- ¹United States National Reconnaissance Office. "The CORONA Story." Declassified/Approved for Release 30 June 2010.
- ²Murbach, M.S., Boronowsky, K.M., and Benton, J.E., et al., "Options for Returning Payloads from the ISS after the Termination of STS Flights," *Proceedings of the 40th AIAA International Conference on Environmental Systems*, Barcelona, Spain, July 11–15, 2010.
- ³Arves, J., Gnau, M., et al., "Overview of the Hybrid Sounding Rocket (HYSR) Project," *Proceedings of the 39th AIAA/ASME/SAE/ASEE Joint Propulsion Conference and Exhibit*, Huntsville, Alabama, July 20-23, 2003.
- ⁴GlobalSecurity.org. "Joint Precision Airdrop System [JPADS]." [www.globalsecurity.org/military/systems/aircraft/systems/jpads.htm. Accessed 03/106/2013]
- ⁵Yakimenko, O. A., Slegers, N. J., and Tiaden, R.A. "Development and Testing of the Miniature Aerial Delivery System Snowflake," *Proceedings of the 20th AIAA Aerodynamic Decelerator Systems Technology Conference and Seminar*, Seattle, Washington, May 4-7, 2009.
- ⁶Yakimenko, O.A., Slegers, N.J., Bourakov, E.A., Hewgley, C.W., Jensen, R.P., Robinson, A.B., Malone, J.R., and Heidt, P.E., "Autonomous Aerial Payload Delivery System "Blizzard"," *Proceedings of the 21st AIAA Aerodynamic Decelerator Systems Technology Conference*, Dublin, Ireland, May 23-26, 2011.
- ⁷Slegers, N., and Yakimenko, O., "Terminal Guidance of Autonomous Parafoils in High Wind to Airspeed Ratios," *Proceedings of the Institution of Mechanical Engineers, Part G: Journal of Aerospace Engineering*, Vol. 225, No. 3, 2011, pp.336-346. doi:10.1243/09544100JAERO749.
- ⁸Yakimenko, O.A., and Slegers, N.J., "Optimization of the ADS Final Turn Maneuver in 2D and 3D," *Proceedings of the 21st AIAA Aerodynamic Decelerator Systems Technology Conference*, Dublin, Ireland, May 23-26, 2011.
- ⁹Yingling, A.J., Hewgley, C.W., Seigenthaler, T.A., and Yakimenko, O.A., "Miniature Autonomous Rocket Recovery System (MARRS)," *Proceedings of the 21st AIAA Aerodynamic Decelerator Systems Technology Conference*, Dublin, Ireland, May 23-26, 2011.
- ¹⁰Zuniga, D., Murbach, M., Leimkuehler, T., Leidich, J., Chiesi, S., "Conceptual Development of a Payload Thermal and Pressure Control System for a Small Payload Quick Return Vehicle," *Proceedings of the 40th AIAA International Conference on Environmental Systems*, Barcelona, Spain, July 11–15, 2010.
- ¹¹Mulloy, C.C., Tiaden, R.D, and Yakimenko, O.A., "The 2nd Generation of Safety Fans GUI," *Proceedings of the 21st AIAA Aerodynamic Decelerator Systems Technology Conference*, Dublin, Ireland, May 23-26, 2011.
- ¹²Benton, J.E., *Miniaturization, Integration, Flight Testing, and Performance Analysis of a Scalable Autonomous GPS-Guided Parafoil System for Targeted Payload Return*, MS Thesis, San Jose State University, San Jose, CA, June, 2012.
- ¹³Corley, M.S., and Yakimenko, O.A., "Computation of the Safety Fans for Multistage Aerodelivery Systems," *Proceedings of the 20th AIAA Aerodynamic Decelerator Systems Technology Conference and Seminar*, Seattle, WA, May 4-7 2009.